Time-serial Assessment of Drug Combination Interventions in a Mouse Model of Colorectal Carcinogenesis Using Optical Coherence Tomography

Libertas Academica
FREEDOM TO RESEARCH

Supplementary Issue: Animal Models of Cancer Biology

Susan LeGendre-McGhee[1], Photini S. Rice[1], R. Andrew Wall[2], Kyle J. Sprute[1], Ramireddy Bommireddy[3], Amber M. Luttman[2], Raymond B. Nagle[4], Edward R. Abril[3], Katrina Farrell[5], Chiu-Hsieh Hsu[6], Denise J. Roe[3,6], Eugene W. Gerner[7], Natalia A. Ignatenko[3,7] and Jennifer K. Barton[1–3]

[1]Department of Biomedical Engineering, University of Arizona, Tucson, AZ, USA. [2]College of Optical Sciences, University of Arizona, Tucson, AZ, USA. [3]University of Arizona Cancer Center, University of Arizona, Tucson, AZ, USA. [4]Department of Pathology, University of Arizona, Tucson, AZ, USA. [5]Department of Chemistry and Biochemistry, University of Arizona, Tucson, AZ, USA. [6]Mel and Enid Zuckerman College of Public Health, University of Arizona, Tucson, AZ, USA. [7]Department of Cellular and Molecular Medicine, University of Arizona, Tucson, AZ, USA.

ABSTRACT: Optical coherence tomography (OCT) is a high-resolution, nondestructive imaging modality that enables time-serial assessment of adenoma development in the mouse model of colorectal cancer. In this study, OCT was utilized to evaluate the effectiveness of interventions with the experimental antitumor agent α-difluoromethylornithine (DFMO) and a nonsteroidal anti-inflammatory drug sulindac during early [chemoprevention (CP)] and late stages [chemotherapy (CT)] of colon tumorigenesis. Biological endpoints for drug interventions included OCT-generated tumor number and tumor burden. Immunochistochemistry was used to evaluate biochemical endpoints [Ki-67, cleaved caspase-3, cyclooxygenase (COX)-2, β-catenin]. *K-Ras* codon 12 mutations were studied with polymerase chain reaction-based technique. We demonstrated that OCT imaging significantly correlated with histological analysis of both tumor number and tumor burden for all experimental groups ($P < 0.0001$), but allows more accurate and full characterization of tumor number and burden growth rate because of its time-serial, nondestructive nature. DFMO alone or in combination with sulindac suppressed both the tumor number and tumor burden growth rate in the CP setting because of DFMO-mediated decrease in cell proliferation (Ki-67, $P < 0.001$) and *K-RAS* mutations frequency ($P = 0.04$). In the CT setting, sulindac alone and DFMO/sulindac combination were effective in reducing tumor number, but not tumor burden growth rate. A decrease in COX-2 staining in DFMO/sulindac CT groups (COX-2, $P < 0.01$) confirmed the treatment effect. Use of nondestructive OCT enabled repeated, quantitative evaluation of tumor number and burden, allowing changes in these parameters to be measured during CP and as a result of CT. In conclusion, OCT is a robust minimally invasive method for monitoring colorectal cancer disease and effectiveness of therapies in mouse models.

KEYWORDS: colorectal cancer, optical coherence tomography, mouse model, α-difluoromethylornithine, sulindac

SUPPLEMENT: Animal Models of Cancer Biology

CITATION: LeGendre-McGhee et al. Time-serial Assessment of Drug Combination Interventions in a Mouse Model of Colorectal Carcinogenesis Using Optical Coherence Tomography. *Cancer Growth and Metastasis* 2015:8(S1) 63–80 doi:10.4137/CGM.S21216.

TYPE: Original Research

RECEIVED: May 19, 2015. **RESUBMITTED:** July 5, 2015. **ACCEPTED FOR PUBLICATION:** July 7, 2015.

ACADEMIC EDITOR: Marc D. Basson, Editor in Chief

PEER REVIEW: Four peer reviewers contributed to the peer review report. Reviewers' reports totaled 874 words, excluding any confidential comments to the academic editor.

FUNDING: Research reported in this publication was supported by the National Cancer Institute of the National Institutes of Health under award numbers R01CA109835, R01CA157595, and P50CA095060. The content is solely the responsibility of the authors and does not necessarily represent the official views of the National Institutes of Health. The authors confirm that the funder had no influence over the study design, content of the article, or selection of this journal.

COMPETING INTERESTS: Eugene W. Gerner has ownership interest in Cancer Prevention Pharmaceuticals, Inc., Tucson, AZ. Other authors disclose no potential conflicts of interest.

CORRESPONDENCE: barton@u.arizona.edu

Paper subject to independent expert blind peer review. All editorial decisions made by independent academic editor. Upon submission manuscript was subject to anti-plagiarism scanning. Prior to publication all authors have given signed confirmation of agreement to article publication and compliance with all applicable ethical and legal requirements, including the accuracy of author and contributor information, disclosure of competing interests and funding sources, compliance with ethical requirements relating to human and animal study participants, and compliance with any copyright requirements of third parties. This journal is a member of the Committee on Publication Ethics (COPE).

Published by Libertas Academica. Learn more about this journal.

Introduction

Colorectal cancer (CRC) is the third leading cancer with respect to incidence and death rates in both men and women in the United States, responsible for 136,830 new cancer cases and 50,310 deaths in 2014.[1] The slow development of CRC over a period of 10–20 years and extensive documentation of common genetic alterations involved in disease progression make CRC a viable target for chemopreventive and chemotherapeutic interventions. In evaluating treatment methodologies for CRC, targeting of the adenomatous polyposis coli (*APC*) gene is of particular interest, as mutation of this gene results in the initiation of the adenoma–carcinoma sequence, and has been found in 70%–80% of human CRC cases.[2,3] The mutant *APC* gene activates the Wnt-signaling pathway, leading to the induction of enzymes regulating cell growth and inflammation, such as the polyamine biosynthetic enzyme ornithine decarboxylase (ODC),[4,5] and the key isoenzymes converting arachidonic acid to prostaglandins, cyclooxygenases 1 and 2 (COX-1 and COX-2).[6–8] Although directly targeting APC with chemopreventive or chemotherapeutic compounds remains difficult, targeting the downstream effectors of Wnt-signaling pathway ODC and cyclooxygenases has been effective in inhibiting colorectal carcinogenesis in animal models and human investigations. The irreversible inhibitor of ODC, α-difluoromethylornithine (DFMO), has been successfully applied to suppress intestinal polyamine levels and

tumor formation in experimental models of colon carcinogenesis as well as in a randomized colon cancer prevention trail.[9–13] The nonsteroidal anti-inflammatory drug (NSAID) sulindac, which exhibits both anti-COX-1 and COX-2 activities, as well as induces cellular polyamine catabolism and export, was also reported to be an effective chemoprevention (CP) agent in both human and murine CRCs.[14–17]

Combinations of DFMO with NSAIDs, such as aspirin, peroxicam, and selective COX-2 inhibitors, have shown antitumor efficacy with possible additive or synergistic mechanisms.[18–22] Furthermore, combined DFMO/sulindac treatment has effectively suppressed colon cancer cell growth and survival responses in vitro and prevented colorectal adenoma formation in a mouse.[22–24] The highly significant efficacy of a combination of DFMO and sulindac has been observed in a randomized double-blind, placebo-controlled phase III trial for colorectal adenoma prevention.[25] These studies, along with the findings from numerous COX-2 inhibitor (coxib) trials[26–28] and the latest randomized celecoxib versus DFMO/celecoxib trail completed in patients with familial adenomatous polyposis (FAP) by Lynch et al,[29] provide important evidence that early neoplasia in the colon can be pharmacologically inhibited/delayed and that polyamines and prostaglandins are valid therapeutic targets in the management of early colorectal neoplasia.

A limitation of current human and rodent investigations of agents acting in a chemopreventive (before tumor formation) and chemotherapeutic (after tumor formation) manner is the challenge of time-serially tracking disease progression within an individual subject. Human studies have been limited to one or two imaging time points, making it impossible to determine the growth rate of adenoma under different treatment regimens. While most previous small animal studies have relied on tumor counts following euthanasia and colon explant, we were particularly interested in tracking tumor number and volume over time, in order to monitor the individual colon tumor growth rates. Also, when performing chemotherapy (CT) studies, the typical lack of information on the number and size of tumors at the start of CT makes exact determination of the chemotherapeutic effect in an individual animal impossible to compute. Thus, to enable time-serial examination of the colon for CP and CT treatment assessment, a nondestructive imaging modality is required.

In the azoxymethane (AOM)-induced CRC mouse model, adenomas develop in the distal colon, which is accessible to high-resolution endoscopic imaging techniques. In this study, we rely on simple, rapid mapping of the distal colon with the cross-sectional imaging modality optical coherence tomography (OCT), which has been miniaturized for the investigation of the distal 30 mm of the mouse colon. Although investigations of disease status in mice using whole-body imaging methods such as magnetic resonance imaging[30] and computed tomography[31] have been conducted, adenomas less than 5 mm in diameter are usually too small to be detected. High-resolution versions of these imaging instruments have met with some success in imaging large adenoma in small animal colon, but remain limited in the ability to detect smaller adenoma, are relatively expensive, and slow.[32] Visual inspection of the distal mouse colon with white-light endoscopes is possible,[33,34] but quantitative evaluation of adenoma size requires a labor- and expertise-dependent process. OCT, on the other hand, is a high-resolution, minimally invasive imaging modality that may be an effective alternative for analyzing disease progression. OCT uses low levels of reflected near-infrared light to form an image with high resolution (2–20 μm) and reasonable penetration depth (1–2 mm).[35] In addition, image acquisition is fully automated and rapid. In vivo studies in human subjects have shown that OCT is capable of delineating the layers of healthy colon,[36,37] detecting adenoma and carcinoma,[37] and differentiating between dysplastic and hyperplastic polyps.[38] OCT is ideal for providing time-serial evaluation of disease progression and therapy, as evidenced by longitudinal studies in the eye (eg, glaucomatous progression)[39] and blood vessels (eg, response to an absorbable scaffold).[40] Furthermore, previous research in our laboratory has developed and applied both dual-modality[41–43] and ultrahigh resolution[44–46] OCT endoscopy systems in mouse models of CRC, demonstrating the ability of OCT to time-serially image individual mice and track disease progression in the distal 30 mm of the colon. Through time-serial imaging, additional parameters such as tumor burden growth rate can be extracted, which is not possible with the current destructive methods.

The present study tests the hypothesis that the OCT is an effective method for monitoring colorectal disease and will be useful for the assessment of efficacy of drug treatments. This hypothesis was tested through time-serial imaging of disease progression in the AOM-induced mouse model of sporadic CRC using an endoscopic spectral-domain OCT system. The study is also aimed to examine the efficacy of DFMO and low-dose sulindac when treatments were applied either before or after adenoma detection (CP or chemotherapeutic regimes) in the same animal model of CRC. Gross photos and histological sections served as gold standard confirmation of disease at the final imaging time point.

Materials and Methods

Endoscopic spectral domain optical coherence tomography system. The design of the endoscopic OCT system implemented in this study has been previously described in detail.[46] Briefly, ultrahigh resolution is achieved using a superluminescent diode light source (Superlum Broadlighter) centered at 890 nm with a 150 nm full-width at half-maximum bandwidth. A 50:50 coupler splits the source optical power into a reference arm and a sample arm. The sample arm consists of a 2 mm diameter endoscope with focusing optics at the tip. The focusing optics include a custom lens assembly coupled into a rod prism to achieve a side-firing endoscope.

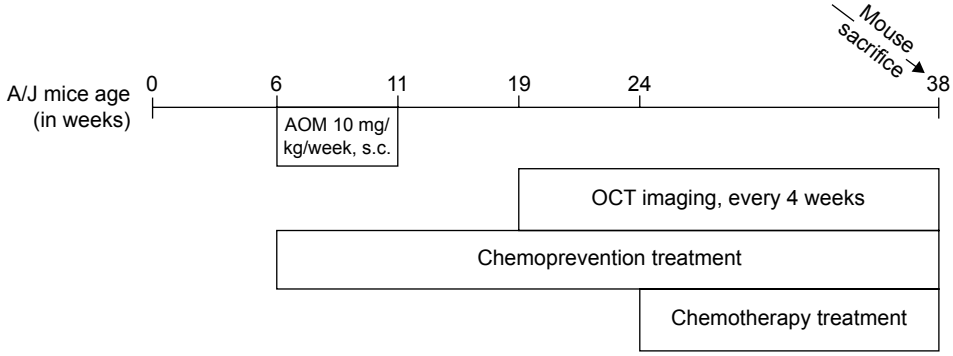

Figure 1. Schematic representation of the experimental protocol.

The endoscope optics are enclosed in a 2 mm diameter glass tube for protection during imaging. Linear and rotation actuators control the lateral and angular position of the endoscope optics inside the glass envelope. Backscattered light from the reference and sample arms recombine at the 50:50 coupler, and interference is detected by a custom-built CCD-based spectrometer. A total of 5000 sampled spectra are reconstructed and combined to form the resultant 30 mm longitudinal × 2 mm deep images (5000 × 1024 pixels) with 5 µm longitudinal and 3.5 µm axial resolution.

Animal model. The commonly used AOM-induced mouse model of sporadic CRC was employed, using a carcinogen-susceptible A/J mouse strain. AOM (10 mg/kg body weight) was purchased from Sigma-Aldrich Chemicals and was administered to mice subcutaneously (sc) once a week for five weeks, starting at six weeks of age. One hundred fourteen A/J mice (Stock #000646), purchased from Jackson Laboratory, were initially enrolled in the study. The experimental protocol for the study is presented in Figure 1. Each experimental group (CP and CT) consisted of two categories of mice (AOM and saline) and four treatment subgroups (no drug, DFMO, sulindac, DFMO/sulindac). Eighty-one mice were weighed and injected with AOM (10 mg/kg body weight, sc; Sigma-Aldrich Chemicals) to induce carcinogenesis. AOM was administered once a week for five weeks, starting at six weeks of age. The remaining 33 mice received saline of equivalent volume following the same dosing schedule. The mice in the AOM and saline no drug groups were used as experimental controls in both the CP and the CT experiments. Treatment with DFMO (Dow Chemical Company,), 1% in water, and/or sulindac (Sigma-Aldrich Chemicals), 100 ppm in AIN 93G food (Harlan Laboratories Inc), was initiated concurrently with AOM induction for the CP group (at six weeks of age), whereas treatment was initiated at 24 weeks of age for the CT experimental group in order to allow adenomas to develop. See Table 1 for the number of mice included in each of the experimental and treatment groups. All mice were housed by the University of Arizona Animal Care on a 12:12 hour light/dark cycle with free access to water and food during the study. All protocols were approved by the University of Arizona Institutional Animal Care and Use Committee.

Imaging protocol. The mice were first imaged ten weeks following AOM induction, and subsequently imaged monthly for four additional months. Total study duration from receipt of the mice to euthanasia was approximately eight months. Twenty-four hours prior to imaging, mice were fasted and

Table 1. Distribution of mice in experimental and treatment groups.

EXPERIMENTAL GROUP	TREATMENT AGENT	NUMBER OF MICE	
		AOM	SALINE
Both	No drug	13 [11] (9)	3 [3] (3)
CP	DFMO 1% in water	13 [11] (11)	5 [4] (4)
	Sulindac 100 ppm in food	10 [7] (7)	3 [3] (2)
	DFMO 1%/sulindac 100 ppm	11 [7] (4)	7 [3] (0)
CT	DFMO 1% in water	12 [12] (10)	7 [4] (4)
	Sulindac 100 ppm in food	9 [9] (6)	3 [3] (3)
	DFMO 1%/sulindac 100 ppm	13 [9] (7)	5 [4] (3)
	Total count:	81 [66] (54)	33 [24] (19)

Notes: First number is mice assigned to experimental and treatment groups. Square brackets denote the number utilized in data analysis (survived to at least 25 weeks for CP or 29 weeks for CT), and parenthesis denote the number of mice that survived through the entire experiment to 38 weeks.
Abbreviations: CP, chemoprevention; CT, chemotherapy.

given Pedialyte® in place of water to clear the colon. Mice were weighed, anesthetized with either 2.6% Avertin solution ip or a mixture of ketamine (0.33 mg/mL, 100 mg/kg) and xylazine (0.033 mg/mL, 10 mg/kg) ip. The colon was then gently flushed with 3–9 mL of warm saline, and the endoscope was coated with a biocompatible water-based lubricant and inserted approximately 32 mm. For all mice, 30 mm longitudinal OCT images were collected at eight different positions spaced 45° apart. Imaging of each mouse took approximately five minutes and required no user intervention.

Tissue acquisition and histology. Following the final imaging time point, the mice were euthanized with CO_2 gas and 30 mm of colorectal tissue was excised for histological processing. Excised colons were opened longitudinally, adhered flat to Whatman paper, gross photos were obtained, and the tissue was fixed in 10% formalin. The fixed colons were embedded in paraffin, longitudinal sections were obtained every 250 μm, and the sections were stained with Hematoxylin and Eosin. A blinded observer analyzed the histological sections to determine the number and maximal width of discrete adenoma per mouse. The gross photos of the excised colons and the results of histological analysis provided gold standard confirmation of the final OCT imaging time point.

Image analysis protocol. OCT image features associated with normal colon tissue and adenoma have been previously verified, and 95% sensitivity to adenoma has been demonstrated.[38] The features of normal colon include consistent mucosal thickness, consistent signal attenuation with image depth, and visible tissue boundaries. Features of adenoma include thickened regional mucosa and/or moderate-to-marked protrusion of mucosa to more than twice the average regional thickness, moderate-to-marked signal attenuation, and faint or obscured tissue boundaries.[38] All eight images for each mouse at each time point (4560 images total) were visually analyzed by a nonblinded observer using the above objective criteria to determine the number of discrete adenoma per mouse. Adenoma size was determined as the maximal width of discrete adenoma identified in the OCT images. Discrete adenoma volume was determined using the aforementioned size value. Owing to the 45° spacing between images, complete characterization of asymmetrical lesions is highly unlikely. As such, spherical volumes were assumed in the calculation of adenoma volume. The size measurements and discrete volumes were then used to calculate total tumor burden (sum of discrete adenoma volumes per mouse at each time point). All measurements were recorded for statistical analysis and comparison with histology. The observer who scored the raw images was different from the blinded observer who scored the histology slides.

Immunohistochemistry and scoring. Colon sections from three animals per each experimental group were processed for immunohistochemistry (IHC) analysis. IHC was performed using the automated Ventana platform from Ventana Medical Systems (VMS) using a streptavidin DAB detection kit from VMS. Tissue was cut to 3 μm thickness and baked at 65°C for 30 minutes before staining. The tissue was stained for proliferation marker Ki-67, apoptosis marker cleaved caspase-3, Wnt-signaling marker β-catenin, and inflammation marker COX-2. For Ki-67, a rabbit monoclonal primary antibody (Leica Biosystems) was used at a dilution of 1:100, with a secondary antibody (biotinylated IgG mouse anti-rabbit from Vector Laboratories Ltd) at a dilution of 1:100, both antibodies were incubated for 30 minutes. Cleaved caspase-3 (Cell Signaling Technology, Inc.), a rabbit monoclonal antibody, was used at a dilution of 1:8000 and incubated for 60 minutes, with a mouse anti-rabbit IgG secondary antibody used at a dilution of 1:100 (Vector Laboratories Ltd) incubated for 30 minutes. For β-catenin, a rabbit monoclonal antibody (Cell Signaling Technology, Inc.) was used at a dilution of 1:300, incubated for 60 minutes followed by a mouse anti-rabbit IgG secondary used at a dilution of 1:100 (Vector Laboratories Ltd) incubated for 30 minutes. The COX-2 antibody was purchased from VMS in a prediluted form and used directly on the tissue, and a mouse anti-rabbit IgG secondary (Vector Laboratories Ltd) was used at a dilution of 1:100 and incubated for 30 minutes. The appropriate positive control tissue was used for each antibody assay. Analysis of the Ki-67 and cleaved caspase-3 staining was done by manually counting the number of positively stained cells in the crypts directly adjacent to the muscularis in 50 colonic crypts per slide. The slides stained for COX-2 and β-catenin were read by an experienced pathologist (RBN) with 30 years of experience, who was blinded to treatment categories. The results are presented as a long score based on the sum of intensity of staining multiplied by the percent of stained tissue area. The following scoring criteria were used: 0, no staining; 1+, weak diffuse staining (may contain stronger intensity in <10% of the cells); 2+, moderate staining in 10%–90% of the cells, and 3+, more than 90% of the cells stained with strong intensity. Staining for all biomarkers was analyzed in three mice from each treatment group except for AOM-sulindac and AOM-DFMO/sulindac groups in CT category where scoring from two mice per group was obtained.

Restriction fragment length polymorphism analysis of mouse *K-Ras* gene codon 12 mutations. DNA was isolated from paraffin-embedded colon tissue slides using Qiagen FFPE kit (QIAGEN Inc.). Specific primers were designed to create a BstNI restriction site at codon 12 of the mouse *K-ras* exon 1. The wild-type primer sequence AAA CTT GTG GTG GTT GGA GCT GGT was modified to create BstN1 restriction site (a G->C change made at codon 11, 3 bp from the 3′ end, bolded underlined below). The following primers were used for the polymerase chain reaction (PCR): 5′-AAA CTT GTG GTG GTT GGA **C**CT and 3′-TCT ATC GTA GGG TCA TAC TC. PCR was performed on identical amounts of DNA (100 ng) and 10 mM primer concentration in a 25 μL reaction using puReTaq™ Ready-To-Go™PCR Beads (Amersham Biosciences Corp.).

Twenty microliters of the PCR product were digested with BstN1 restriction endonuclease for two hours at 60°C, and restriction enzyme-digested and undigested PCR products were resolved on a 3% NuSieve:agarose (3:1) gel stained with ethidium bromide. A mutation at codon 12 of the *K-RAS* gene (G to C transition) changes the sequence of the BstNI site, so it is no longer recognizable by the BstNI enzyme and preserves the fragment size (98 bp) (Supplementary Fig. 1).

Statistical analysis methods. Statistical comparison of OCT data between experimental and treatment groups was performed for weight gain, number of tumors, tumor burden growth rate, and IHC staining. Data for all saline category treatment groups within an experimental group were combined, as values did not vary significantly. Statistical analysis of tumor number and tumor burden growth rate only included the AOM-treated mice. All measurement time points were included for the CP experimental group, whereas only time points following treatment initiation at 24 weeks of age were included for the CT experimental group. Statistical analysis of weight gain and tumor burden growth rate was performed by fitting a linear regression line to the values measured across time for individual mice. The analysis of the number of tumors was based on the maximum observed number of tumors over the entire study duration or at time of death for individual mice. Mice that died before the end of the experiment were excluded from these analyses if they did not have at least two measurements to allow slope estimation or one measurement of maximum value. Thus, in the CP experiment, five mice (all AOM categories) that died before week 21 were excluded from weight gain analysis and tumor number analysis, and nine AOM mice that died before week 25 were excluded from the tumor burden growth rate analysis. In the CT experiment, 10 mice that died before week 29 were excluded from the weight gain analysis, six AOM mice that died before week 29 were excluded from tumor burden growth rate analysis, and four AOM mice that died before week 25 were excluded from tumor number analysis. The number of animals in each category included in tumor burden growth rate analysis is shown in square brackets in Table 1. The number of mice surviving to the final time point is shown in parentheses in Table 1.

In the analysis of weight gain, the effects of AOM versus saline, DFMO treatment (presence or absence), and sulindac treatment (presence or absence) were assessed using a three-way ANOVA. As a three-way interaction between these variables was found to be not significant, it was removed from the model and all two-way interactions were assessed. When a two-way interaction was statistically significant ($P < 0.05$), stratified analyses were performed. In the analysis of tumor burden growth rate, only AOM-treated mice were included in a two-way ANOVA, with stratified analyses performed if appropriate. The number of tumors was analyzed using Poisson regression, with assessment of interaction as outlined above. All *P*-values reported are two-sided and are not adjusted for multiple comparisons.

In order to verify the accuracy of OCT, statistical analyses of the final OCT time point and histology with respect to the number of tumors and tumor burden were performed. The data from all mice with corresponding histology were included in these analyses. The data for the AOM and saline-no drug groups were used in both the CP and CT comparisons. When animals were sacrificed before the end of the study, the values observed at the time of sacrifice were used in the analyses. The correlation between the OCT and histology tumor burden measurements was assessed using the Pearson correlation coefficient and confirmed using the nonparametric Spearman correlation coefficient. The distribution of the number of tumors was compared using a Fisher's exact test. Differences in the mean values for tumor burden and the number of tumors were tested using the nonparametric Wilcoxon signed-rank test.

Statistical analysis of IHC staining was performed to evaluate the treatment effects and differences between treatment groups in terms of the number of positively stained cells (for Ki-67 and cleaved caspase-3) or staining score (for β-catenin and COX-2). Each analysis was done using score results from different animals (number of animals specified in the tables) per each treatment group. For Ki-67 and cleaved caspase-3, the mean number of positively stained cells and the associated standard deviation were presented and Poisson regression with overdispersion was performed to evaluate the treatment effects and the differences between treatment groups in the number of positively stained cells. For β-catenin and COX-2, the average score of IHC staining and the associated standard deviation were presented and linear regression was performed to evaluate the treatment effects and the differences between treatment groups in the staining score. For both Poisson and linear regression, Tukey's post hoc test was performed to adjust for multiple comparisons while evaluating the differences between groups.

Fisher's exact test was employed to test for the difference in the occurrence of *K-RAS* mutations between the different treatment groups. All *P*-values reported are two-sided and are not adjusted for multiple comparisons.

Results

Time-serial analysis of disease progression in OCT. The OCT system yielded high-resolution images of murine colonic morphology with clear distinction between tissue types such as the mucosa, submucosa, and muscularis propria. Furthermore, the micron-scale resolution attained by this system allowed relevant markers of disease progression to be tracked. OCT can image about 1 mm deep in mouse colon tissue, sufficient to image through the entire normal colon and smaller adenoma. An example OCT image series for one mouse over the five imaging time points is presented in Figure 2, along with corresponding final time point histology. In the first image (Fig. 2A), a colonic lesion portraying several of the characteristics consistent with adenoma, such

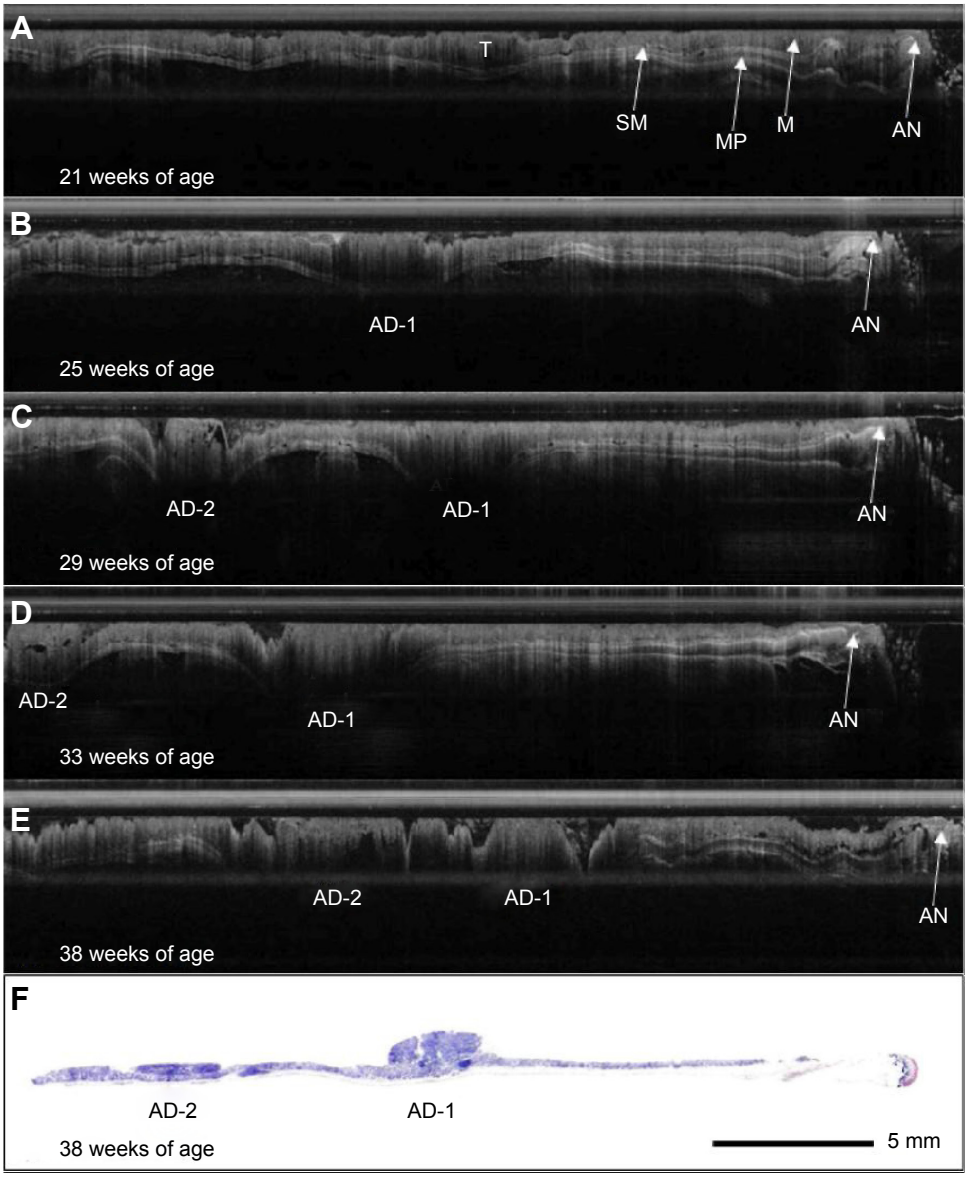

Figure 2. Time-serial OCT image series. OCT image series for a single mouse at a single rotation over time. (**A**)–(**E**) 30 mm lateral OCT images obtained at each imaging time point and (**F**) corresponding histology. OCT shows excellent delineation of colon structures, as well as the development of disease. The development of two adenoma (AD-1 and AD-2) is evident. OCT image contrast was adjusted for improved visibility.
Abbreviations: AN, anus; M, mucosa; SM, submucosa; MP, muscularis propria; T, abnormally thickened mucosal area.

as regional mucosal thickening and marked signal attenuation, is evident. Additionally, tissue boundaries are faint compared to adjacent normal colon. However, the lesion does not meet the mucosal protrusion of more than twice the average regional thickness criteria. As such, it would not be counted as an adenoma. In contrast, the same lesion is depicted in the second image (Fig. 2B), portraying all of the characteristics consistent with adenoma. In the third through fifth images (Fig. 2C, D, and E, respectively), an additional lesion with characteristics consistent with adenoma appears in the proximal end of the images. As time progresses, both lesions significantly increase in size. The corresponding histological section (Fig. 2F) confirms the presence of adenoma at the suspected locations.

Accuracy of OCT. The final time point OCT and histology means and standard errors for the number of tumors and tumor burden for both experimental groups are depicted in Table 2. The results for the number of tumors were very similar between OCT and histology, whereas the tumor burden measured by OCT was consistently higher than that measured by histology. Both Pearson and Spearman correlation analyses determined that highly significant correlations existed between the OCT and histology measurements for both the number of tumors and tumor burden for both experimental groups (all $P < 0.0001$). The statistical analyses comparing the mean number of tumors showed no statistically significant differences between the OCT and histology data for either experimental group ($P = 0.24$ for CP and $P = 0.69$

Table 2. Comparison of OCT and histology data for the number of tumors and tumor burden.

	NUMBER OF TUMORS		TUMOR BURDEN (IN mm^3)	
	MEAN (SE)	*P*-VALUE	MEAN (SE)	*P*-VALUE
CP				
OCT	2.39 (0.44)	0.24	39.05 (9.09)	0.0073
Histology	2.18 (0.39)		24.59 (6.29)	
CT				
OCT	3.89 (0.41)	0.69	82.88 (17.11)	0.0026
Histology	3.87 (0.39)		56.18 (8.95)	

Notes: All mice that had histology data available were included in these analyses. The data for the AOM and saline no drug groups were included in both the CP and CT analyses.
Abbreviations: CP, chemoprevention; CT, chemotherapy.

for CT). However, significant differences in the tumor burden values for OCT versus histology were found in both the CP and CT experimental groups ($P = 0.0073$ and $P = 0.0026$, respectively). Overall, OCT was determined to have 89.02% sensitivity to adenoma, and only 12.57% of the total number of tumors identified were false positives (21 out of 167).

CP experimental group. For the CP experimental group, OCT image analysis resulted in the finding that 100% of the mice in the no drug group developed adenomas over the course of the study, whereas prevalence was reduced to 72.7% in the DFMO group, 85.7% in the sulindac group, and 22.2% in the DFMO/sulindac group. The value of treatment with DFMO and/or sulindac is further depicted in Figure 3, showing a drastic reduction in the average number of tumors and

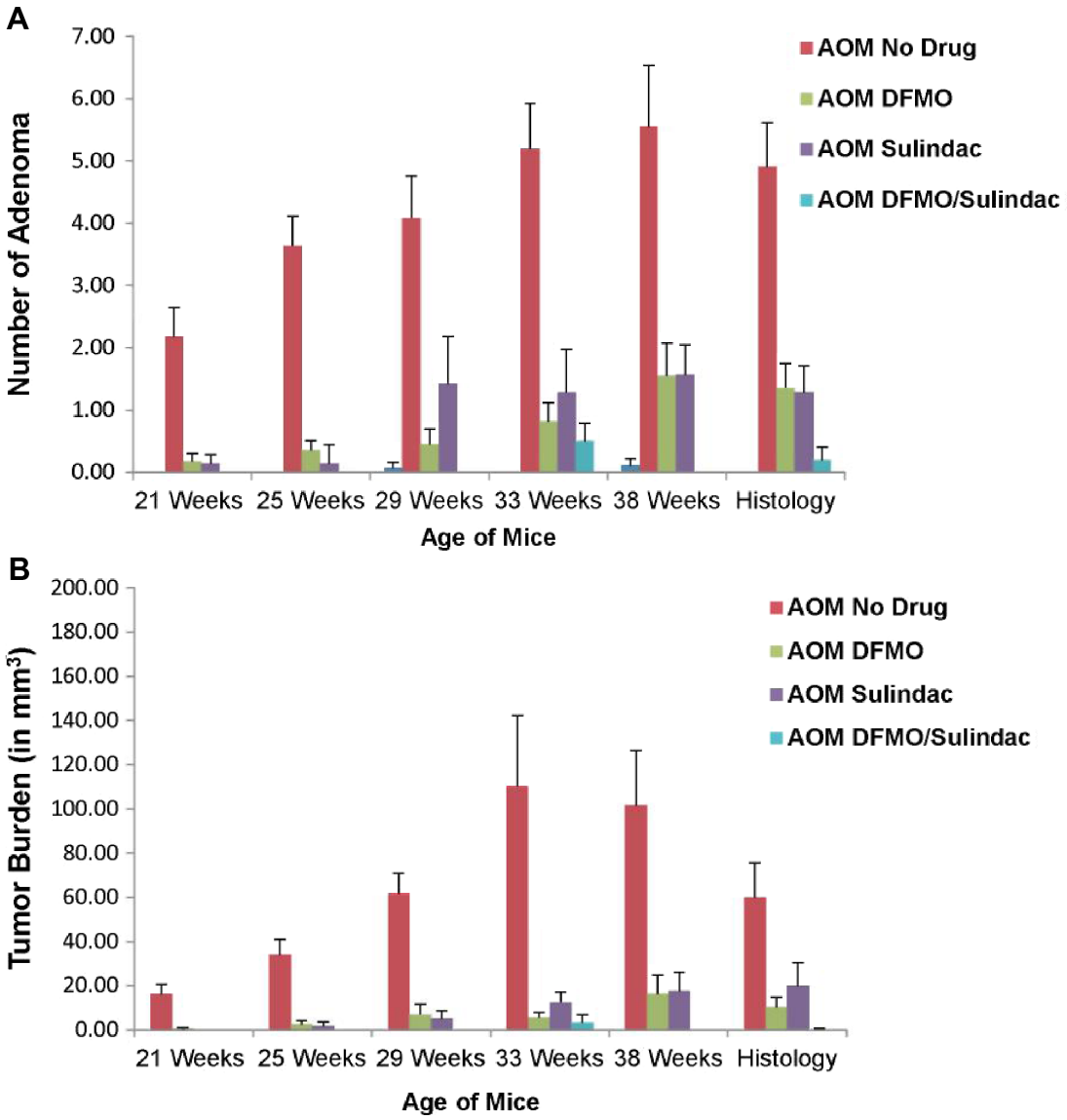

Figure 3. Chemoprevention experimental group time-serial plots of average number of tumors and average tumor burden. Depicted above are the plots for average number of tumors per mouse (**A**) and the average tumor burden per mouse (**B**). The number of mice in each group is as follows (AOM-no drug, AOM-DFMO, AOM-sulindac, AOM-DFMO/sulindac): 21 weeks (11,11,7,7), 25 weeks (11,11,7,7), 29 weeks (11,11,7,7), 33 weeks (10,11,7,7), 38 weeks (9,11,7,4), and histology (11,11,7,5). All available histological sections were included in the analyses, resulting in an increased number of mice at histology than at the 38-week time point.

average tumor burden growth rate per mouse over time in the DFMO and sulindac treatment groups. Statistical analysis of the AOM-treated mice by two-way ANOVA revealed a significant effect of DFMO ($P < 0.0001$), sulindac ($P = 0.0003$), and the DFMO/sulindac combination ($P < 0.0001$) on the maximum number of tumors observed when compared with the AOM-no drug group. A statistically significant interaction between the drugs was not found ($P = 0.57$), nor was there a significant difference between DFMO alone versus sulindac alone ($P = 0.51$). Analysis of tumor burden growth rate by two-way ANOVA found that DFMO and sulindac interacted at a statistically significant level ($P = 0.0039$), with a statistically significant decrease compared with AOM-no drug ($P < 0.0001$). Subsequent stratified analyses determined that treatment with either drug alone significantly reduced tumor burden growth rate in the absence of the other drug ($P = 0.0002$ for DFMO, $P = 0.0030$ for sulindac). There was no statistically significant difference in tumor burden growth rate in the effect of DFMO alone versus sulindac alone ($P = 0.83$). Data are compiled in Table 3.

IHC analysis of colonic tissues from different treatment groups (three slides/group) revealed that in the CP setting both DFMO and sulindac suppressed cell growth as single agents or in combination as assessed by Ki-67 IHC (Fig. 4A). Statistical analysis of Ki-67-positively stained cells shows that DFMO treatment was more effective than sulindac in the inhibition of cell proliferation (AOM-no drug vs AOM-DFMO, $P < 0.001$, AOM-no drug vs AOM-sulindac, $P = 0.03$, and AOM-no drug vs DFMO/sulindac, $P < 0.0001$) (Table 4A). None of the pairwise comparisons of cleaved caspase-3 positively stained cells between AOM-no drug and CP treatment groups reached statistical significance (Table 5A). The analysis of pattern and level of expression of COX-2 protein in colon tissue samples showed epithelial staining with the localization of COX-2 protein in lamina propria cells, in crypts, and inflammatory cells, but there was no localization of COX-2 in dysplastic epithelial cells within the AOM-induced tumors (Fig. 4B).

In the AOM-DFMO/sulindac group, a 3.75-fold decrease in the mean COX-2 intensity score in the crypts was observed, but this difference was not statistically significant because of a high variation between the samples (Table 6A). β-catenin staining was not affected by any treatment (Supplementary Tables 1 and 2). The only difference was found in β-catenin staining of adenomas where the intensity score was higher in cytoplasm and lower in membrane compared to the normal mucosa (Fig. 4C, Supplementary Tables 1C and 2C, $P < 0.0001$ for both).

The restriction fragment length polymorphism (RFLP) analysis of the mutational status of the *K-Ras* gene (codon 12) identified that 37.5% of samples in AOM-no drug group and 40% in AOM-sulindac group carried the mutation in codon 12 of *K-Ras* gene. On the contrary, DFMO treatment prevents occurrence of *K-Ras*-mutations in the AOM-DFMO treatment group (Table 7, $P = 0.0429$ is statistically significant) as it suppresses cell proliferation.[47] The AOM-DFMO/sulindac group had a lower percent *of K-Ras* mutation (7.69%) compared to no drug and sulindac groups (Table 7).

CT experimental group. For the CT experimental group, the average number of tumors and average tumor burden growth rate per treatment group over time are depicted in Figure 5, showing a less dramatic effect of the drugs. A statistically significant interaction between DFMO and sulindac was not found with respect to either maximum

Table 3. Comparison of treatment group means and standard errors for weight gain, maximum number of tumors, and tumor burden growth rate.

A. TREATMENT GROUP	CHEMOPREVENTION					
	WEIGHT GAIN		MAXIMUM NUMBER OF TUMORS		TUMOR BURDEN GROWTH RATE	
	MEAN SLOPE	SE	MEAN	SE	MEAN SLOPE	SE
AOM-no drug	0.11	0.02	5.54	0.12	6.53	0.72
AOM-sulindac	0.04	0.03	1.86*	0.28	1.10*	0.95
AOM-DFMO	0.10	0.02	1.46*	0.23	0.84*	0.76
AOM-DFMO/sulindac	−0.11*	0.02	0.33*	0.58	0.56*	0.89
B. TREATMENT GROUP	**CHEMOTHERAPY**					
	WEIGHT GAIN		MAXIMUM NUMBER OF TUMORS		TUMOR BURDEN GROWTH RATE	
	MEAN SLOPE	SE	MEAN	SE	MEAN SLOPE	SE
AOM-no drug	0.02	0.04	5.92	0.12	7.09	2.14
AOM-sulindac	0.07	0.05	4.11*	0.16	2.02	2.36
AOM-DFMO	0.00	0.04	4.67	0.13	5.52	2.04
AOM-DFMO/sulindac	−0.21*	0.04	3.00*	0.18	2.32	2.36

Notes: Depicted is the mean data for (**A**) the CP and (**B**) the CT experimental groups (*$P < 0.01$ when compared with AOM-no drug).

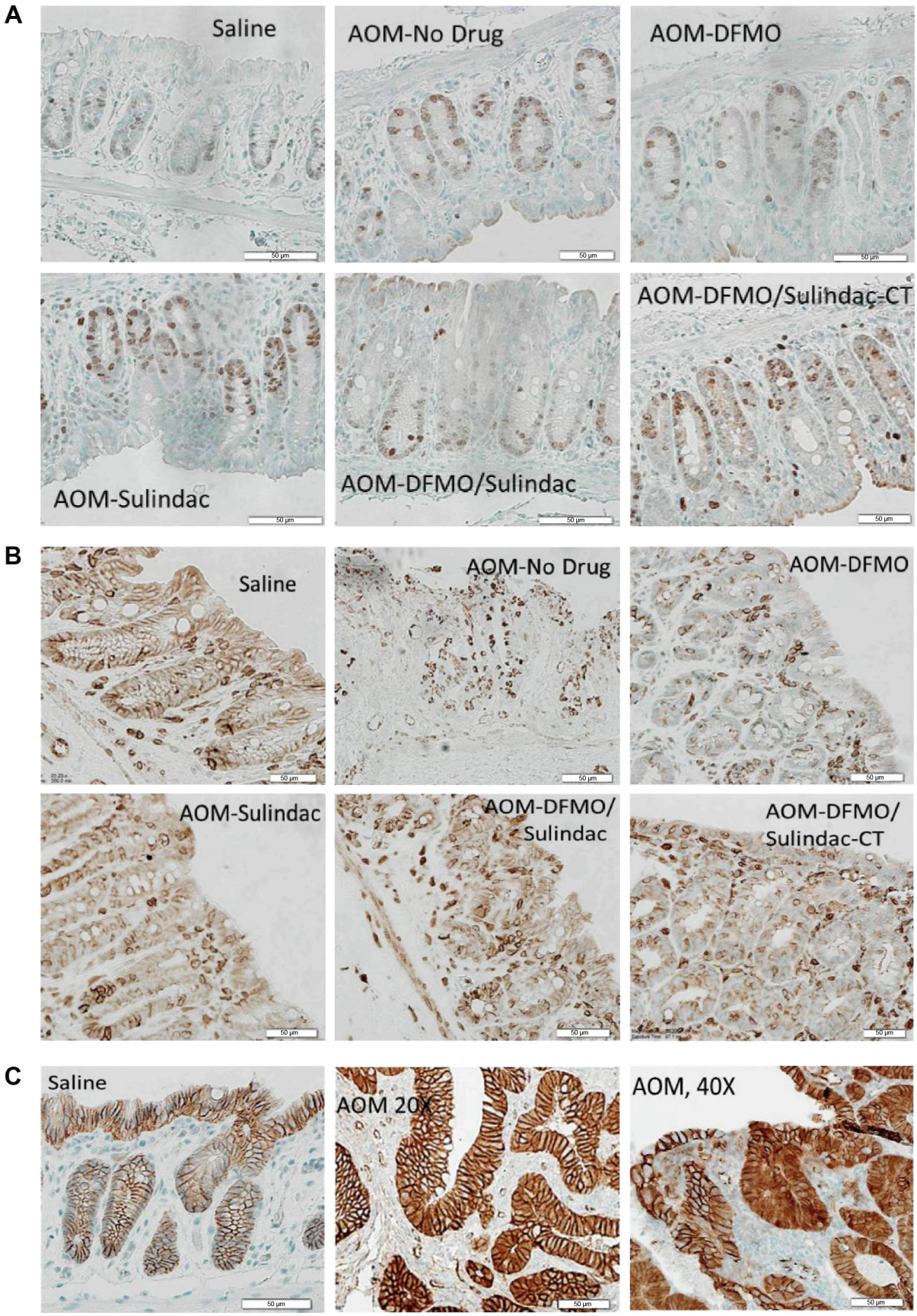

Figure 4. Examples of IHC staining of Ki-67, COX-2, and β-catenin. (**A**) Ki-67 positive cells in chemoprevention groups; (**B**) COX-2 staining in selected treatment groups. All sections are from CP treatment groups, except when specified (CT group—CT); 20× magnification; (**C**) β-catenin staining in untreated group (saline) and AOM-no drug group.

Table 4. IHC scores for Ki-67 staining. (**A**) Mean number (mean) of positively stained cells, number of slides analyzed (*N*), and the associated standard deviation (SD). (**B**) Evaluation of treatment effects for the experimental groups.

A.			
EXPERIMENTAL GROUP	**GROUP***	**MEAN (*N*)**	**SD**
Both	Saline	457.67 (3)	67.42
CP	AOM-no drug	657.33 (3)	77.51
	AOM-DFMO	415.67 (3)[a]	60.47
	AOM-sulindac	475.00 (3)[b]	87.68
	AOM-DFMO/sulindac	371.00 (3)[c]	35.93
CT	AOM-no drug	657.33 (3)	77.51
	AOM-DFMO	870.33 (3)	105.56
	AOM-sulindac	667.00 (2)	32.53
	AOM-DFMO/sulindac	550.50 (2)[d]	21.92

B.		
COMPARISONS	**MEAN (*N*)**	**SD**
AOM		
No	457.67 (3)	67.42
Yes	568.58 (19)	181.27
P-value[e]	0.29	
DFMO		
No	554.91 (11)	119.02
Yes	552.00 (11)	221.52
P-value	0.97	
Sulindac		
No	600.25 (12)	200.57
Yes	497.30 (10)	121.15
P-value	0.15	
Treated w/DFMO or sulindac		
No (AOM only)	657.33 (3)	77.51
Yes (AOM + DFMO/sulindac)	551.94 (16)	191.73
P-value	0.35	

Notes: Scores mean values (mean), number of slides analyzed (*N*), and standard deviation (SD) for all experimental groups. *Pairwise comparisons significance: CP—AOM-no drug vs treatment: [a]$P < 0.001$, [b]$P = 0.03$, [c]$P < 0.0001$; CT—AOM-DFMO vs AOM-DFMO/sulindac: [d]$P < 0.001$. [e]Derived from a Poisson regression model with adjustment for potential overdispersion.

Table 5. IHC scores for cleaved caspase-3 staining. (**A**) Mean number (mean) of positively stained cells, number of slides analyzed (*N*), and the associated standard deviation (SD). (**B**) Evaluation of treatment effects for the experimental groups.

A.			
EXPERIMENTAL GROUP	**GROUP***	**MEAN (*N*)**	**SD**
Both	Saline	3.33 (3)	3.06
CP	AOM-no drug	2.00 (3)	3.46
	AOM-DFMO	9.67 (3)	3.51
	AOM-sulindac	1.67 (3)	0.56
	AOM-DFMO/sulindac	5.33 (3)	0.58
CT	AOM-no drug	2.00 (3)	3.46
	AOM-DFMO	7.33 (3)	3.21
	AOM-sulindac	3.00 (2)	1.41
	AOM-DFMO/sulindac	6.00 (2)	2.83

B.		
COMPARISONS	**MEAN (*N*)**	**SD**
AOM		
No	3.33 (3)	3.06
Yes	5.05 (19)	3.60
P-value[a]	0.47	
DFMO		
No	2.45 (11)	2.25
Yes	7.18 (11)	2.93
P-value	<0.001	
Sulindac		
No	5.58 (12)	4.27
Yes	3.90 (10)	2.18
P-value	0.30	
Treated w/DFMO or sulindac		
No (AOM only)	2.00 (3)	3.46
Yes (AOM + DFMO/sulindac)	5.63 (16)	3.42
P-value	0.13	

Notes: Scores mean values (mean), number of slides analyzed (*N*), and standard deviation (SD) for all experimental groups. *None of the pairwise comparisons in the evaluation of differences between AOM-no drug and treatment groups is significant. [a]Derived from a Poisson regression model with adjustment for potential overdispersion. Turkey method was used to adjust for multiple comparisons.

number of tumors ($P = 0.80$) or tumor burden growth rate ($P = 0.68$). Statistical analysis by two-way ANOVA revealed a significant effect of sulindac ($P = 0.0072$) but not DFMO ($P = 0.07$) on the maximum number of tumors per mouse. DFMO and sulindac in combination statistically significantly reduced the tumor number in treated animals compared to AOM-no drug animals ($P < 0.01$), but there was no difference between the combination versus sulindac alone ($P = 0.20$). Neither sulindac ($P = 0.07$) nor DFMO ($P = 0.73$) were found to significantly reduce tumor burden growth rate. Data are compiled in Table 3.

The analysis of IHC staining for Ki-67 and cleaved caspase-3 showed that neither agent nor their combination were able to significantly reduce cell proliferation or stimulate apoptosis in treated animals compared to AOM-no drug mice when the agents were applied after tumor initiation (Tables 4A and 5A). But when individual treatment groups were compared, DFMO/sulindac combination group had reduced Ki-67 staining compared to AOM-DFMO group (Table 4A, $P < 0.001$). Treatments did not have any statistically significant effect on the expression levels or intracellular distribution of β-catenin in the normal tissue (Supplementary Tables 1A and 2A). Analysis

Table 6. IHC scores for COX-2 staining in colon crypt area. (**A**) Average score of IHC staining (mean), number of slides analyzed (*N*), and the associated standard deviation (SD). (**B**) Evaluation of treatment effects for the experimental groups.

A.			
EXPERIMENTAL GROUP	**GROUP***	**MEAN (*N*)**	**SD**
Both	Saline	280 (3)	17.32
CP	AOM-no drug	185 (3)	161.79
	AOM-DFMO	300 (3)	0
	AOM-sulindac	200 (3)	100
	AOM-DFMO/sulindac	53.33 (3)[a,b]	41.63
CT	AOM-no drug	185 (3)	161.79
	AOM-DFMO	123.33 (3)	127.41
	AOM-sulindac	70 (2)	70.71
	AOM-DFMO/sulindac	40 (2)[c]	0

B.		
COMPARISONS	**MEAN (*N*)**	**SD**
AOM		
No	280 (3)	17.32
Yes	147.63 (19)	119.96
P-value[d]	<0.05	
DFMO		
No	194.09 (11)	114.56
Yes	137.27 (11)	124.91
P-value	0.24	
Sulindac		
No	222.08 (12)	115.63
Yes	98 (10)	90.65
P-value	<0.01	
Treated w/DFMO or sulindac		
No (AOM only)	185 (3)	161.79
Yes (AOM + DFMO/sulindac)	140.63 (16)	115.96
P-value	0.54	

Notes: Scores mean values (mean), number of slides analyzed (*N*), and standard deviation (SD) for all experimental groups. *Pairwise comparisons significance: CP—saline vs AOM-DFMO/sulindac. [a]$P < 0.01$; CP-AOM-DFMO vs AOM-DFMO/sulindac, [b]$P < 0.001$; CP—AOM-DFMO vs CT-AOM-DFMO/sulindac, [c]$P < 0.01$. [a–c]Tukey method is used to adjust for multiple comparisons. [d]Derived from a linear regression model.

of *K-Ras* mutation in different treatment groups showed the decrease in the percent of identified *K-Ras* mutations in all treatment groups compared to AOM-no drug group but these results did not reach statistical significance (Table 7, CT).

Discussion

Minimally invasive, high-resolution optical imaging techniques have demonstrated their ability to identify early microscopic changes associated with neoplasia.[48] Optical imaging modalities, such as OCT, confocal microscopy, fluorescence imaging, and multiphoton microscopy (MPM), are ideal for the early detection of colon as well as other (eg, ovarian) cancers.[32–46,49–52] We have recently shown that imaging of mouse models with OCT, fluorescence imaging, and MPM at multiple time points is possible and allows for the detection of microscopic and macroscopic changes in the tissue with disease progression.[52–54]

In this study, we applied endoscopic OCT time-serial imaging to determine the effectiveness of DFMO and low-dose sulindac treatments in a mouse model of CRC. We tested two treatment regimens: chemopreventive and chemotherapeutic, and corroborated the final time point endoscopy results with IHC analysis of colon tissue for biochemical assessment of drug interventions. Endoscopic OCT images of each mouse were obtained at five different time points and utilized to determine the number of adenomas and tumor burden. This study was novel for two reasons. First, it evaluated multiple treatment regimes at multiple times, whereas previous research using these drugs have only evaluated one time point of one treatment regime (DFMO,[10,11] sulindac,[14–16] or the combination of DFMO and sulindac[23,24]). A second novel aspect of this study is that our endoscopic OCT system enabled nondestructive imaging, which allows us to determine the number of tumors and tumor burden as a function of time. Thus, analysis of tumor burden slope, or growth rate, could be conducted. As shown in Figure 5, mice in the CT experimental group did not start with the same number of tumors or tumor burden, so nondestructive imaging was crucial for proper statistical analysis of the effects of DFMO and sulindac in a chemotherapeutic setting.

Table 7. Percent of *K-Ras* mutation for the AOM-treated mice.

EXPERIMENTAL CATEGORY	GROUP	NUMBER OF SAMPLES ANALYZED	%(N) OF MUTANT *K-RAS*	*P*-VALUE FOR THE DIFFERENCE BETWEEN AOM-NO DRUG AND TREATMENT GROUPS
Both	Saline	15	13.33 (2)	
CP	AOM-no drug	8	37.5 (3)	
	AOM-DFMO	9	0 (0)	0.0429
	AOM-sulindac	5	40.00 (2)	0.9282
	AOM-DFMO/sulindac	13	7.69 (1)	0.2528
CT	AOM-no drug	8	37.5 (3)	
	AOM-DFMO	27	14.81 (4)	0.3117
	AOM-sulindac	13	15.38 (2)	0.3254
	AOM-DFMO/sulindac	6	16.67 (1)	0.6804

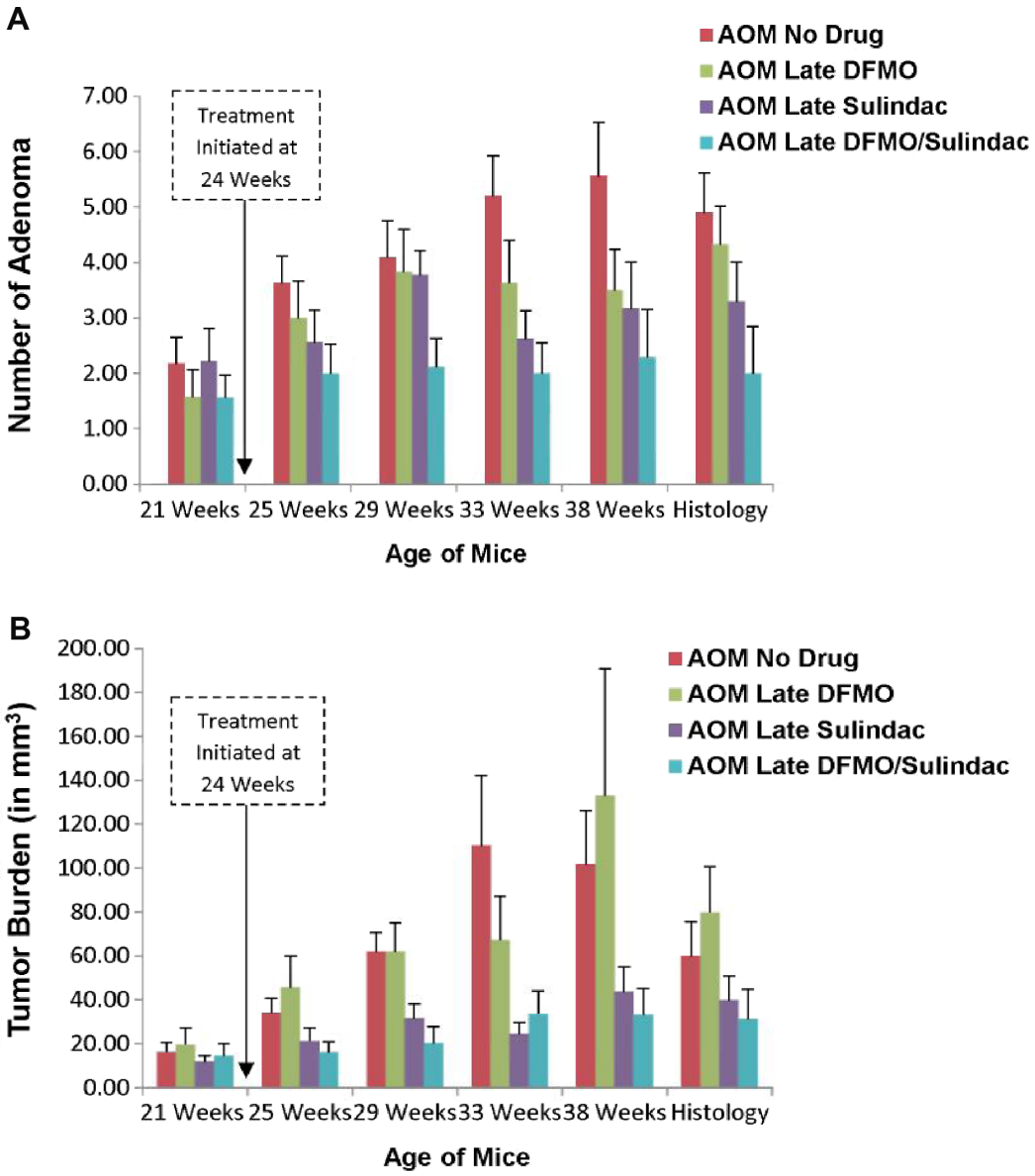

Figure 5. CT experimental group time-serial plots of average number of tumors and average tumor burden. Depicted above are the plots for average number of tumors per mouse (**A**) and the average tumor burden per mouse (**B**). The number of mice in each group is as follows (AOM-no drug, AOM late DFMO, AOM late sulindac, AOM late DFMO/sulindac): 21 weeks (11,12,9,9), 25 weeks (11,12,9,9), 29 weeks (11,12,9,9), 33 weeks (10,11,8,9), 38 weeks (9,10,6,7), and histology (11,12,7,7). All available histological sections were included in the analyses, resulting in an increased number of mice at histology than at the 38-week time point.

OCT accuracy and measurement error. Our OCT system clearly delineated the architectural features of healthy colonic tissue, including the mucosa, submucosa, and muscularis propria, and differentiated between normal tissue and adenoma (see Fig. 2). Imaging with OCT is far more rapid than with a white-light endoscope; no colon insufflation or special expertise is required, a series of images is obtained in less than 5 minutes, and images are a known constant scale for easy measurement of tumor size. Comparison of final imaging time point data with histology showed a significant correlation between measurements taken by OCT and histology. Also, adenoma detection based on OCT image analysis is highly accurate. However, OCT consistently estimated a larger tumor burden than histology, because of errors in adenoma sizing most likely from sampling error, tissue distortion, suboptimal image quality in a few cases, and histological processing. OCT images were only obtained every 45°, which may lead to sampling error in size estimation. Insertion of the endoscope causes adenoma to compress, violating the assumption of a spherical tumor. In some OCT images of highly diseased colons, the image quality was degraded by residual feces or blood, making it more difficult to discern adenoma from residual debris, or distinguish individual adenoma from multiple adenomas in close proximity to each other. Finally, histological processing is known to dehydrate and shrink tissue samples, so histological measurements are expected

to be smaller than those obtained in vivo. In one controlled study, the average OCT layer thickness was 19% larger than histology.[55] However, even with these limitations, our protocol was able to correctly identify adenoma with a sensitivity of 89.02%, with only 12.57% of the adenomas counted being false positives. This finding compares similarly with our previous studies on accuracy of adenoma detection,[46] which found a sensitivity of 95% and false positive rate of 15.56%.

Efficacy of DFMO and sulindac treatments. DFMO acts to prevent intestinal carcinogenesis by a mechanism involving the irreversible inhibition of the polyamine biosynthetic enzyme ODC, suppression of genes involved in cell migration cell–cell communication,[47] and depletion of tissue thymidine pools.[56] In contrast, the NSAID sulindac has been shown to inhibit the activities of the two isoforms (COX-1 and COX-2) of cyclooxygenase enzyme, as well as induces apoptosis through both COX-dependent[14] and COX-independent mechanisms.[17]

Our current findings of biological endpoints (tumor number and tumor burden) and cancer biomarkers prove that DFMO is an effective CP treatment modality for reducing both the number of tumors and tumor burden growth rate. The lack of an interaction between DFMO and sulindac and the lower average number of tumors observed in the DFMO/sulindac combination group suggests that these drugs may combine additively to further reduce the number of adenoma that develop. With respect to tumor burden growth rate, no effect of DFMO was found, but there was a nearly significant ($P = 0.07$) effect of sulindac. Based on these results, it appears that DFMO is most likely to have a significant effect on inhibiting carcinogenesis when applied during the initiation stage, whereas sulindac may be effective in both the initiation and promotion stages.

IHC analyses served as independent markers associated with cancer treatment. The IHC for Ki-67 protein, which is elevated in proliferating cells and correlates with the clinical course of the disease, shows that the number of Ki-67 positively stained cells was low in DFMO and DFMO/sulindac treated colon tissues in the CP setting (Table 4). Ki-67 scoring analysis suggests that DFMO acts as the more efficient inhibitor of cell proliferation than sulindac.

When treatments were started after adenomas became visible by OCT (CT setting), sulindac alone showed effectiveness in reducing the colon tumor number, but not tumor burden. In CT setting, DFMO and DFMO/sulindac groups had elevated levels of apoptosis by cleaved caspase-3 positive cells staining (Table 5A), although comparison between AOM-no drug and these treatment groups did not reach statistical significance.

Furthermore, we performed IHC staining of the colon tissues from different treatment groups for COX-2 protein. COX-2 is involved in initiation and promotion of malignancy in different cancers, and elevated expression of COX-2 protein and prostaglandin levels have been reported in human adenomas and carcinomas of the colon.[57,58] In our study, COX-2 expression was used as a marker of the treatment efficacy with sulindac, a nonselective COX-2 inhibitor. We found the most significant suppression of the COX-2 protein expression in DFMO/sulindac combination groups of both CP and CT treatment settings.

We also measured the level and subcellular localization of β-catenin in the colon tissue samples of animals from different experimental groups. β-catenin is a known transcriptional regulator of the Wnt-signaling pathway. β-catenin is also involved in cell adhesion through its complex with cadherin; therefore, it is important in the development of CRC.[3] In this study, the expression and subcellular localization of β-catenin was not significantly affected by the applied treatments. The only difference was found in adenomas compared to the normal mucosa, such that adenomas had increased cytoplasmic staining and decreased cytoplasmic membranous staining (Fig. 5C and Supplementary Tables 1C and 2C, $P < 0.0001$ for both). Loss of membranous β-catenin staining, significantly less nuclear staining, and elevated cytoplasmic staining have been observed in colonic adenomas of FAP patients resistant to sulindac treatment.[59]

CRC arises as a result of progression from benign colorectal adenoma to malignant carcinoma through accumulation of chromosomal abnormalities, genetic mutations, and epigenetic changes.[2] Because of the reported resistance to sulindac treatment of adenomas that carry mutations in the *K-RAS* oncogene,[59] we measured the mutational status of *K-Ras* in colon samples of control and treated animal in CP and CT groups. Guda et al[60] reported a low (6%) frequency of *K-Ras* activating mutations, located predominantly in exon 1 of *K-Ras* gene, in AOM-treated A/J mice sacrificed at 32 weeks of age. In our study, mice were sacrificed at 38 weeks of age and had higher (37.5%) frequency of *K-Ras* mutations in the AOM-no drug group (Table 7). Treatment with DFMO was effective in preventing the occurrence of *K-Ras* mutations in the CP study (0%, mutations, $P = 0.043$). In the CT setting, there was no statistically significant difference in the occurrence of *K-Ras* mutations between AOM-no drug and treatment groups ($P > 0.05$), although all treatment groups had the lower percent of *K-Ras* mutations compared to AOM-no drug (Table 7). Based on this finding, we concluded that the lack of significant effect of treatments initiated in CT setting may be explained in part by the accumulation of *K-Ras* mutations before the start of treatment.

Agents toxicity in AOM-induced A/J mouse model of colon carcinogenesis. Limitations of the animal model should be considered when translating these findings to human colon cancer prevention and treatment. CRC in human beings can develop as a consequence of alterations in a number of pathways, including the sporadic and FAP-associated adenoma–carcinoma sequence, hereditary nonpolyposis CRC and colonic inflammation-associated cancer.[3] The molecular events associated with colorectal

disease progression include frequent somatic mutations and deletions in tumor-related genes, including *K-RAS, APC*, and p53. In the AOM-induced CRC model, the most frequently found mutation is in the *K-RAS* oncogene, whereas mutations in *APC* and p53 tumor suppressor genes are less common.[60–62] Moreover, in the AOM-treated mouse model, the AOM derivative methylazoxymethanol (MAM) induces DNA adduct formation, leading to genetic alterations in DNA repair genes, TGF-β signaling molecules, β-catenin, and *K-RAS*,[63] resulting in the upregulation of COX-2 and ODC. This carcinogenesis pathway represents the less common genetic alteration in human beings, whereas an estimated 70%–80% of cases are initiated by a mutation in the *APC* gene.[3] Therefore, the effectiveness of treatment with DFMO and sulindac in this mouse model may not be completely comparable with human cases where APC is mutated. The incidence and multiplicity of colonic adenomas are significantly higher in AOM-induced A/J mice compared to AOM-induced C57BL/6 and 129/Sv mouse strains making it a suitable model for CP research. A/J mice metabolize more AOM on average than other strains of mice because of increased activity of CYP2E1 (an enzyme that converts AOM to MAM).[63] The particular susceptibility of A/J mice to AOM could result in liver toxicity, which would compromise the metabolism of sulindac.[64] Finally, treatment in this model was dependent upon animal eating and drinking habits. A decrease in food and water consumption could have limited the ability of DFMO and sulindac to prevent carcinogenesis. Previous research with human subjects has indicated that the extended use of DFMO or NSAIDs causes toxic side effects. For instance, dosage-dependent mild-to-moderate temporary hearing loss is a known toxicity of treatment with DFMO.[12,13,25,65,66] On the other hand, extended NSAID use has been associated with gastrointestinal bleeding, gastrointestinal permeability, and increased risk of cardiovascular events.[67–69] The NSAIDs most likely to be toxic are of the coxib type, which tend to be selective COX-2 inhibitors.[67]

The current study utilized a lower dose of DFMO (1%) and sulindac (100 ppm), compared to doses used in previous studies with a C57BL6 strain.[24] In the present study, a statistically significant reduction in weight gain resulted from the combination of DFMO and sulindac, regardless of experimental or treatment group, and for sulindac alone for mice in the CP group, which were exposed to the agent for a longer period of time than the CT group. Treatment with DFMO alone did not alter the animal weights. It is possible that the mice simply found the taste of the drug-laced food to be disagreeable. It is also possible that A/J mice are more susceptible for the chronic effect of sulindac on the gastrointestinal epithelium than other strains.[64] Although specific evaluations for upper gastrointestinal ulcerations were not performed at necropsy, visual inspection of the mice at each imaging time point and of the excised colons did not reveal any adverse side effects of treatment with DFMO and/or sulindac.

Conclusion and Future Directions

This first application of OCT for tracking colonic disease progression and evaluating chemopreventive and chemotherapeutic agent effectiveness significantly improved upon the current paradigms for evaluating disease progression and agent effectiveness in human and mouse models, allowing time-serial data on an individual subject to be easily and quickly obtained. Furthermore, the design of this study evaluated multiple treatment regimes, enabling the interaction between DFMO and sulindac to be elucidated, as well as the effect of agent timing relative to adenoma formation. In addition, analysis of cancer biomarkers in this study was performed on the same experimental animals and provided the molecular basis for the observed effects of DFMO, sulindac, and its combination.

Our results show that DFMO/sulindac combination can be successfully used as chemopreventive and chemotherapeutic treatments for suppression of colon tumor number. The current study suggests that DFMO is most effective when the treatment is initiated with the start of AOM injections and continues through the initiation, promotion, and progression stages of colon carcinogenesis. Also, in the CP setting, DFMO treatment prevented occurrence of *K-Ras* mutations in the AOM-induced colon cancer model. Therefore, DFMO alone is very effective in suppressing colon carcinogenesis in the chemopreventive setting. Time-serial imaging analysis of the tumor number and tumor burden growth rate in the CT setting confirmed the effectiveness of sulindac treatment in suppressing colon tumor number compared to AOM-no drug or AOM-DFMO CT groups. In previous studies, sulindac was found to be the most effective when given during the promotion/progression stages, attributed to its effect on apoptosis.[70,71] In our study, sulindac was effective in suppressing COX-2 expression, but did not have any effect on apoptosis, evaluated by cleaved caspase-3 staining.

The efficacy of pharmaceuticals administered during surveillance intervals to prevent colon carcinogenesis may depend on whether the agents prevent new adenomas from forming or cause regression of existing adenomas. Future studies could determine if reducing the exposure interval to these agents would retain sufficient anticarcinogenesis activity while reducing the risk of potential toxicities associated with DFMO and/or sulindac. While the currently used endoscopic OCT system was highly capable of obtaining useful measures of tumor count and burden, more accurate measures of adenoma size and shape, and thus tumor burden, could be obtained using a spiral-scanning OCT system that obtains three-dimensional images of the colon. In future studies, we will use a system, similar to the one previously reported.[72] Additionally, future development of endoscopic OCT systems capable of cellular resolutions may enable earlier detection of neoplasia in both

mouse models and human patients, thereby improving the morbidity and mortality rates associated with CRC.

Abbreviations

DFMO, α-difluoromethylornithine; APC, adenomatous polyposis coli; AOM, azoxymethane; COX, cyclooxygenase; DMH, dimethylhydrazine; MAM, methylazoxymethanol; FAP, familial adenomatous polyposis; NSAID, nonsteroidal anti-inflammatory drug; OCT, optical coherence tomography; ODC, ornithine decarboxylase; RFLP, restriction fragment length polymorphism; CP, chemoprevention; CT, chemotherapy.

Acknowledgments

University of Arizona Cancer Center Support Grant (including usage of Shared Resources) P30CA023074.

Author Contributions

Conceived and designed the experiments: SL, EWG, NAI, and JKB. Analyzed the data: SL, PSR, RAW, KJS, RB, AL, CHH, DJR, RBN, ERA, KF, and NAI. Wrote the first draft of the manuscript: SL. Contributed to the writing of the manuscript: PSR, RAW, RB, DJR, NAI, and JKB. Agreed with manuscript results and conclusions: all the authors. Jointly developed the structure and arguments for the paper: SL, EWG, NAI, and JKB. Made critical revisions and approved the final version: all. All the authors reviewed and approved the final manuscript.

REFERENCES

1. American Cancer Society. *Cancer Facts & Figures 2014*. Atlanta: American Cancer Society; 2014.
2. Fearon ER, Vogelstein B. A genetic model for colorectal tumorigenesis. *Cell*. 1990; 61(5):759–767.
3. Fearon ER. Molecular genetics of colorectal cancer. *Annu Rev Pathol*. 2011; 6(479):507.
4. Gerner EW, Meyskens FL Jr. Polyamines and cancer: old molecules, new understanding. *Nat Rev Cancer*. 2004;4(10):781–792.
5. Fultz KE, Gerner EW. APC-dependent regulation of ornithine decarboxylase in human colon tumor cells. *Mol Carcinog*. 2002;34(1):10–18.
6. Fitzpatrick FA. Cyclooxygenase enzymes: regulation and function. *Curr Pharm Des*. 2004;10(6):577–588.
7. Howe LR, Subbaramaiah K, Chung WJ, Dannenberg AJ, Brown AM. Transcriptional activation of cyclooxygenase-2 in Wnt-1-transformed mouse mammary epithelial cells. *Cancer Res*. 1999;59(7):1572–1577.
8. Nunez F, Bravo S, Cruzat F, Montecino M, De Ferrari GV. Wnt/beta-catenin signaling enhances cyclooxygenase-2 (COX2) transcriptional activity in gastric cancer cells. *PLoS One*. 2011;6(4):e18562.
9. Nigro ND, Bull AW, Boyd ME. Inhibition of intestinal carcinogenesis in rats: effect of difluoromethylornithine with piroxicam or fish oil. *J Natl Cancer Inst*. 1986;77(6):1309–1313.
10. Tempero MA, Nishioka K, Knott K, Zetterman RK. Chemoprevention of mouse colon tumors with difluoromethylornithine during and after carcinogen treatment. *Cancer Res*. 1989;49(21):5793–5797.
11. Erdman SH, Ignatenko NA, Powell MB, et al. APC-dependent changes in expression of genes influencing polyamine metabolism, and consequences for gastrointestinal carcinogenesis, in the Min mouse. *Carcinogenesis*. 1999;20(9):1709–1713.
12. Meyskens FL Jr, Gerner EW, Emerson S, et al. Effect of alpha-difluoromethylornithine on rectal mucosal levels of polyamines in a randomized, double-blinded trial for colon cancer prevention. *J Natl Cancer Inst*. 1998;90(16):1212–1218.
13. Love RR, Jacoby R, Newton MA, et al. A randomized, placebo-controlled trial of low-dose alpha-difluoromethylornithine in individuals at risk for colorectal cancer. *Cancer Epidemiol Biomarkers Prev*. 1998;7(11):989–992.
14. Gupta RA, Dubois RN. Colorectal cancer prevention and treatment by inhibition of cyclooxygenase-2. *Nat Rev Cancer*. 2001;1(1):11–21.
15. Beazer-Barclay Y, Levy DB, Moser AR, et al. Sulindac suppresses tumorigenesis in the Min mouse. *Carcinogenesis*. 1996;17(8):1757–1760.
16. Hu Y, Le Leu RK, Young GP. Sulindac corrects defective apoptosis and suppresses azoxymethane-induced colonic oncogenesis in p53 knockout mice. *Int J Cancer*. 2005;116(6):870–875.
17. Babbar N, Ignatenko NA, Casero RA Jr, Gerner EW. Cyclooxygenase-independent induction of apoptosis by sulindac sulfone is mediated by polyamines in colon cancer. *J Biol Chem*. 2003;278(48):47762–47775.
18. Li H, Schut HA, Conran P, et al. Prevention by aspirin and its combination with alpha-difluoromethylornithine of azoxymethane-induced tumors, aberrant crypt foci and prostaglandin E2 levels in rat colon. *Carcinogenesis*. 1999;20(3):425–430.
19. Rao CV, Tokumo K, Rigotty J, Zang E, Kelloff G, Reddy BS. Chemoprevention of colon carcinogenesis by dietary administration of piroxicam, alpha-difluoromethylornithine, 16 alpha-fluoro-5-androsten-17-one, and ellagic acid individually and in combination. *Cancer Res*. 1991;51(17):4528–4534.
20. Reddy BS, Nayini J, Tokumo K, Rigotty J, Zang E, Kelloff G. Chemoprevention of colon carcinogenesis by concurrent administration of piroxicam, a nonsteroidal antiinflammatory drug with D,L-alpha-difluoromethylornithine, an ornithine decarboxylase inhibitor, in diet. *Cancer Res*. 1990;50(9):2562–2568.
21. Jacoby RF, Cole CE, Tutsch K, et al. Chemopreventive efficacy of combined piroxicam and difluoromethylornithine treatment of APC mutant Min mouse adenomas, and selective toxicity against APC mutant embryos. *Cancer Res*. 2000;60(7):1864–1870.
22. Lawson KR, Ignatenko NA, Piazza GA, Cui H, Gerner EW. Influence of K-ras activationon the survival responses of Caco-2 cells to the chemopreventive agents sulindac and difluoromethylornithine. *Cancer Epidemiol Biomarkers Prev*. 2000; 9(11):1155–1162.
23. Zell JA, Ignatenko NA, Yerushalmi HF, et al. Risk and risk reduction involving arginine intake and meat consumption in colorectal tumorigenesis and survival. *Int J Cancer*. 2007;120(3):459–468.
24. Ignatenko NA, Besselsen DG, Stringer DE, Blohm-Mangone KA, Cui H, Gerner EW. Combination chemoprevention of intestinal carcinogenesis in a murine model of familial adenomatous polyposis. *Nutr Cancer*. 2008;60(suppl 1): 30–35.
25. Meyskens FL Jr, McLaren CE, Pelot D, et al. Difluoromethylornithine plus sulindac for the prevention of sporadic colorectal adenomas: a randomized placebo-controlled, double-blind trial. *Cancer Prev Res (Phila)*. 2008;1(1):32–38.
26. Bertagnolli MM, Eagle CJ, Zauber AG, et al; APC Study Investigators. Celecoxib for the prevention of sporadic colorectal adenomas. *N Engl J Med*. 2006; 355(9):873–884.
27. Arber N, Eagle CJ, Spicak J, et al; PreSAP Trial Investigators. Celecoxib for the prevention of colorectal adenomatous polyps. *N Engl J Med*. 2006;355(9):885–895.
28. Baron JA, Sandler RS, Bresalier RS, et al; APPROVe Trial Investigators. A randomized trial of rofecoxib for the chemoprevention of colorectal adenomas. *Gastroenterology*. 2006;131(6):1674–1682.
29. Lynch PM, Burke CA, Phillips R, et al. An international randomised trial of celecoxib versus celecoxib plus difluoromethylornithine in patients with familial adenomatous polyposis. *Gut*. 2015 Mar 19. pii: gutjnl-2014-307235. doi:10.1136/gutjnl-2014-307235. [Epub ahead of print].
30. Achiam MP, Thomsen HS, Rosenberg J. Magnetic resonance colonography in clinical use: how far have we come? *Scand J Gastroenterol*. 2009;44(5):518–526.
31. Halligan S, Taylor SA. CT colonography: results and limitations. *Eur J Radiol*. 2007;61(3):400–408.
32. Koo V, Hamilton PW, Williamson K. Non-invasive in vivo imaging in small animal research. *Cell Oncol*. 2006;28(4):127–139.
33. Miller SJ, Lee CM, Joshi BP, Gaustad A, Seibel EJ, Wang TD. Targeted detection of murine colonic dysplasia in vivo with flexible multispectral scanning fiber endoscopy. *J Biomed Opt*. 2012;17(2):021103.
34. Miller SJ, Heist KA, Feng Y, et al. Multimodal imaging of growth and rapamycin-induced regression of colonic adenomas in APC mutation-dependent mouse. *Transl Oncol*. 2012;5(5):313–320.
35. Drexler W, Fujimoto JG, eds. *Optical Coherence Tomography: Technology and Applications*. Berlin: Springer-Verlag; 2008.
36. Jäckle S, Gladkova N, Feldchtein F, et al. In vivo endoscopic optical coherence tomography of the human gastrointestinal tract—toward optical biopsy. *Endoscopy*. 2000;32(10):743–749.
37. Sivak MV Jr, Kobayashi K, Izatt JA, et al. High-resolution endoscopic imaging of the GI tract using optical coherence tomography. *Gastrointest Endosc*. 2000; 51(4 pt 1):474–479.
38. Testoni PA, Mangiavillano B. Optical coherence tomography in detection of dysplasia and cancer of the gastrointestinal tract and bilio-pancreatic ductal system. *World J Gastroenterol*. 2008;14(42):6444–6452.
39. Na JH, Sung KR, Lee JR, et al. Detection of glaucomatous progression by spectral-domain optical coherence tomography. *Ophthalmology*. 2013;120(7):1388–1395.

40. Zhang YJ, Iqbal J, Nakatani S, et al; ABSORB Cohort B Study Investigators. Scaffold and edge vascular response following implantation of everolimus-eluting bioresorbable vascular scaffold: a 3-year serial optical coherence tomography study. *JACC Cardiovasc Interv*. 2014;7(12):1361–1369.
41. Tumlinson AR, Hariri LP, Utzinger U, Barton JK. Miniature endoscope for simultaneous optical coherence tomography and laser-induced fluorescence measurement. *Appl Opt*. 2004;43(1):113–121.
42. Hariri LP, Tumlinson AR, Besselsen DG, Utzinger U, Gerner EW, Barton JK. Endoscopic optical coherence tomography and laser-induced fluorescence spectroscopy in a murine colon cancer model. *Lasers Surg Med*. 2006;38(4):305–313.
43. Winkler AM, Rice PF, Weichsel J, et al. In vivo, dual-modality OCT/LIF imaging using a novel VEGF receptor-targeted NIR fluorescent probe in the AOM-treated mouse model. *Mol Imaging Biol*. 2011;13(6):1173–1182.
44. Tumlinson AR, Povazay B, Hariri LP, et al. In vivo ultrahigh-resolution optical coherence tomography of mouse colon with an achromatized endoscope. *J Biomed Opt*. 2006;11(6):064003.
45. Winkler AM, Rice PF, Drezek RA, Barton JK. Quantitative tool for rapid disease mapping using optical coherence tomography images of azoxymethane-treated mouse colon. *J Biomed Opt*. 2010;15(4):041512.
46. Hariri LP, Qiu Z, Tumlinson AR, et al. Serial endoscopy in azoxymethane treated mice using ultra-high resolution optical coherence tomography. *Cancer Biol Ther*. 2007;6(11):1753–1762.
47. Ignatenko NA, Zhang H, Watts GS, Skovan BA, Stringer DE, Gerner EW. The chemopreventive agent alpha-difluoromethylornithine blocks Ki-ras-dependent tumor formation and specific gene expression in Caco-2 cells. *Mol Carcinog*. 2004; 39(4):221–233.
48. Tang S, Zhou Y, Ju MJ. Multimodal optical imaging with multiphoton microscopy and optical coherence tomography. *J Biophotonics*. 2012;5(5–6):396–403.
49. Hariri LP, Bonnema GT, Schmidt K, et al. Laparoscopic optical coherence tomography imaging of human ovarian cancer. *Gynecol Oncol*. 2009;114(2):188–194.
50. Hariri LP, Liebmann ER, Marion SL, et al. Simultaneous optical coherence tomography and laser induced fluorescence imaging in rat model of ovarian carcinogenesis. *Cancer Biol Ther*. 2010;10(5):438–447.
51. George R, Michaelides M, Brewer MA, Utzinger U. Parallel factor analysis of ovarian autofluorescence as a cancer diagnostic. *Lasers Surg Med*. 2012;44(4): 282295.
52. Watson JM, Marion SL, Rice PF, et al. In vivo time-serial multi-modality optical imaging in a mouse model of ovarian tumorigenesis. *Cancer Biol Ther*. 2014; 15(1):42–60.
53. Keenan MR, Leung SJ, Rice PS, Wall RA, Barton JK. Dual optical modality endoscopic imaging of cancer development in the mouse colon. *Lasers Surg Med*. 2015;47(1):30–39.
54. Leung SJ, Rice PS, Barton JK. In vivo molecular mapping of the tumor microenvironment in an azoxymethane-treated mouse model of colon carcinogenesis. *Lasers Surg Med*. 2015;47(1):40–49.
55. Bonnema GT, Cardinal KO, McNally JB, Williams SK, Barton JK. Assessment of blood vessel mimics with optical coherence tomography. *J Biomed Opt*. 2007; 12(2):024018.
56. Witherspoon M, Chen Q, Kopelovich L, Gross SS, Lipkin SM. Unbiased metabolite profiling indicates that a diminished thymidine pool is the underlying mechanism of colon cancer chemoprevention by alpha-difluoromethylornithine. *Cancer Discov*. 2013;3(9):1072–1081.
57. Chapple KS, Cartwright EJ, Hawcroft G, et al. Localization of cyclooxygenase-2 in human sporadic colorectal adenomas. *Am J Pathol*. 2000;156(2):545–553.
58. Eberhart CE, Coffey RJ, Radhika A, Giardiello FM, Ferrenbach S, DuBois RN. Up-regulation of cyclooxygenase 2 gene expression in human colorectal adenomas and adenocarcinomas. *Gastroenterology*. 1994;107(4):1183–1188.
59. Keller JJ, Offerhaus GJ, Drillenburg P, et al. Molecular analysis of sulindac-resistant adenomas in familial adenomatous polyposis. *Clin Cancer Res*. 2001;7(12): 4000–4007.
60. Guda K, Upender MB, Belinsky G, et al. Carcinogen-induced colon tumors in mice are chromosomally stable and are characterized by low-level microsatellite instability. *Oncogene*. 2004;23(21):3813–3821.
61. Erdman SH, Wu HD, Hixson LJ, Ahnen DJ, Gerner EW. Assessment of mutations in Ki-*ras* and *p53* in colon cancers from azoxymethane- and dimethylhydrazine-treated rats. *Mol Carcinog*. 1997;19(2):137–144.
62. Takahashi M, Wakabayashi K. Gene mutations and altered gene expression in azoxymethane-induced colon carcinogenesis in rodents. *Cancer Sci*. 2004;95(6): 475–480.
63. Sohn OS, Fiala ES, Requeijo SP, Weisburger JH, Gonzalez FJ. Differential effects of CYP2E1 status on the metabolic activation of the colon carcinogens azoxymethane and methylazoxymethanol. *Cancer Res*. 2001;61(23):8435–8440.
64. Bissahoyo A, Pearsall RS, Hanlon K, et al. Azoxymethane is a genetic background-dependent colorectal tumor initiator and promoter in mice: effects of dose, route, and diet. *Toxicol Sci*. 2005;88(2):340–345.
65. Croghan MK, Aickin MG, Meyskens FL. Dose-related alpha-difluoromethylornithine ototoxicity. *Am J Clin Oncol*. 1991;14(4):331–335.
66. McLaren CE, Fujikawa-Brooks S, Chen WP, et al. Longitudinal assessment of air conduction audiograms in a phase III clinical trial of difluoromethylornithine and sulindac for prevention of sporadic colorectal adenomas. *Cancer Prev Res (Phila)*. 2008;1(7):514–521.
67. Salvo F, Fourrier-Réglat A, Bazin F, et al; Investigators of Safety of Non-Steroidal Anti-Inflammatory Drugs: SOS Project. Cardiovascular and gastrointestinal safety of NSAIDs: a systematic review of meta-analyses of randomized clinical trials. *Clin Pharmacol Ther*. 2011;89(6):855–866.
68. Giardiello FM, Yang VW, Hylind LM, et al. Primary chemoprevention of familial adenomatous polyposis with sulindac. *N Engl J Med*. 2002;346:1054–1059.
69. Zell JA, Pelot D, Chen WP, McLaren CE, Gerner EW, Meyskens FL. Risk of cardiovascular events in a randomized placebo-controlled, double-blind trial of difluoromethylornithine plus sulindac for the prevention of sporadic colorectal adenomas. *Cancer Prev Res (Phila)*. 2009;2(3):209–212.
70. Boolbol SK, Dannenberg AJ, Chadburn A, et al. Cyclooxygenase-2 overexpression and tumor formation are blocked by sulindac in a murine model of familial adenomatous polyposis. *Cancer Res*. 1996;56(11):2556–2560.
71. Samaha HS, Kelloff GJ, Steele V, Rao CV, Reddy BS. Modulation of apoptosis by sulindac, curcumin, phenylethyl-3-methylcaffeate, and 6-phenylhexyl isothiocyanate: apoptotic index as a biomarker in colon cancer chemoprevention and promotion. *Cancer Res*. 1997;57(7):1301–1305.
72. Tsai TH, Potsaid B, Tao YK, et al. Ultrahigh speed endoscopic optical coherence tomography using micromotor imaging catheter and VCSEL technology. *Biomed Opt Express*. 2013;4(7):1119–1132.

Supplementary Materials

Animal deaths. Twenty-four of 114 mice were excluded from analysis because of early death, and only 73 mice lived through the entirety of the study. A variety of factors may have contributed to deaths, including the anesthetic Avertin, AOM induction, and random environmental factors. Extended use of Avertin has been shown to result in acute toxicities and death.[1] Following the premature death of several mice, we switched to ketamine/xylazine anesthesia. Evaluation of several of the AOM-treated mice that died noted liver disease. Previous research showed that injection with a modestly higher dose of AOM (ie, 20 mg/kg body weight) resulted in the death of all mice within one week.[64] AOM at the incorrect concentration may have been received, as nearly all mice in one group

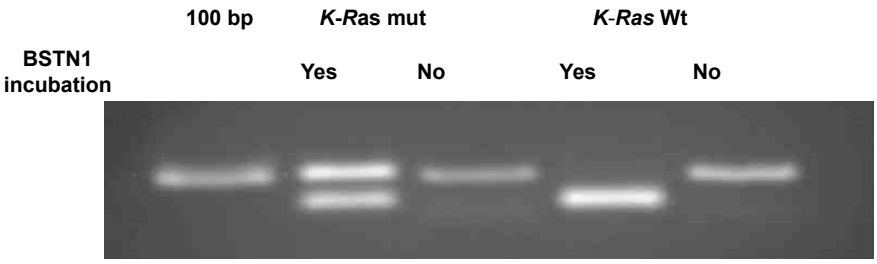

Supplementary Figure 1. Example RFLP analysis result for the detection of mutant *K-Ras* codon 12.

Supplementary Table 1. IHC scores of β-catenin–membrane staining. (**A**) Average score of IHC staining in normal tissue (mean), number of slides analyzed (*N*), and the associated standard deviation (SD). (**B**) Average score of IHC staining in tumors (mean), number of slides analyzed (*N*), and the associated standard deviation (SD). (**C**) Evaluation of treatment effects for the experimental groups. Scores mean values (mean), number of slides analyzed (*N*), and standard deviation (SD) for all experimental groups.

A.

EXPERIMENTAL GROUP	GROUP	MEAN (*N*)	SD
Both	Saline	290 (3)	17.32
CP	AOM-no drug	300 (3)	0
	AOM-DFMO	300 (3)	0
	AOM-sulindac	293.33 (3)	11.55
	AOM-DFMO/sulindac	300 (2)	0
CT	AOM-no drug	300 (3)	0
	AOM-DFMO	300 (3)	0
	AOM-sulindac	275 (2)	35.36
	AOM-DFMO/sulindac	300 (1)	0

B.

EXPERIMENTAL GROUP	GROUP	MEAN (*N*)	SD
Both	Saline	n/a	17.32
CP	AOM-no drug	200 (2)	0
	AOM-DFMO	n/a	n/a
	AOM-sulindac	200 (1)	0
	AOM-DFMO/sulindac	300 (1)	0
CT	AOM-no drug	300 (3)	0
	AOM-DFMO	183.33 (3)	28.87
	AOM-sulindac	250 (1)	0
	AOM-DFMO/sulindac	300 (1)	0

C.

COMPARISONS	MEAN (N)	SD
AOM		
No	290 (3)	17.32
Yes	270.38 (26)	46.95
P-value[a]	0.48	
DFMO		
No	270.00 (15)	40.36
Yes	275.00 (14)	50.95
P-value	0.76	
Sulindac		
No	265.88 (17)	52.21
Yes	281.67 (12)	3.15
P-value	0.34	
Tumor		
No	295.00 (20)	13.18
Yes	222.22 (9)	50.69
P-value	<0.0001	
Treated w/DFMO or sulindac		
No (AOM only)	260.00 (5)	54.77
Yes (AOM + DFMO/sulindac)	272.86 (21)	46.06
P-value	0.57	

Notes: Tukey method is used to adjust for multiple comparisons. None of the pairwise comparisons are significant. [a]Derived from a linear regression model.

Supplementary Table 2. IHC scores of β-catenin–cytoplasm staining. (**A**) Average score of IHC staining in normal tissue (mean), number of slides analyzed (*N*), and the associated standard deviation (SD). (**B**) Average score of IHC staining in tumors (mean), number of slides analyzed (*N*), and the associated standard deviation (SD). (**C**) Evaluation of treatment effects for the experimental groups. Scores mean values (mean), number of slides analyzed (*N*), and standard deviation (SD) for all experimental groups.

A.

EXPERIMENTAL GROUP	GROUP	MEAN (*N*)	SD
Both	Saline	100 (3)	10
CP	AOM-no drug	136.67 (3)	47.26
	AOM-DFMO	100 (3)	0
	AOM-sulindac	100 (3)	0
	AOM-DFMO/sulindac	100 (2)	0
CT	AOM-no drug	136.67 (3)	47.26
	AOM-DFMO	100 (3)	0
	AOM-sulindac	75 (2)	35.36
	AOM-DFMO/sulindac	100 (1)	0

B.

EXPERIMENTAL GROUP	GROUP	MEAN (*N*)	SD
Both	Saline	n/a	
CP	AOM-no drug	252.5 (2)	67.18
	AOM-DFMO	n/a	n/a
	AOM-sulindac	300 (1)	0
	AOM-DFMO/sulindac	250 (1)	0
CT	AOM-no drug	300 (3)	0
	AOM-DFMO	183.33 (3)	47.26
	AOM-sulindac	200 (1)	0
	AOM-DFMO/sulindac	220 (1)	0

C.

COMPARISONS	MEAN (*N*)	SD
AOM		
No	100 (3)	0
Yes	145.58 (26)	69.34
P-value[a]	0.25	
DFMO		
No	144.33 (15)	76.79
Yes	137.14 (14)	57.44
P-value	0.77	
Sulindac		
No	139.12 (17)	60.63
Yes	143.33 (12)	77.97
P-value	0.87	
Tumor		
No	103 (20)	23.86
Yes	225 (9)	53.15
P-value	<0.0001	
Treated w/DFMO or sulindac		
No (AOM only)	183 (5)	79.18
Yes (AOM + DFMO/sulindac)	136.67 (21)	65.75
P-value	0.16	

Notes: Tukey method is used to adjust for multiple comparisons. None of the pairwise comparisons are significant. [a]Derived from a linear regression model.

died after one or two doses of AOM. Furthermore, the deaths ceased when an alternate lot of AOM was used. Several of the mice in the DFMO and/or sulindac treatment groups were among those that died prior to completion of the study. Owing to the above confounders, however, it was impossible to determine whether treatment contributed to those deaths.

Animal weight analysis. There was a statistically significant interaction between DFMO and sulindac in both experimental groups ($P = 0.0025$ for CP, $P = 0.0032$ for CT), regardless of whether the animals were AOM- or saline-treated ($P = 0.32$ and 0.27, respectively). Owing to this interaction, the combination of DFMO and sulindac resulted in a significant decrease in weight gain (both $P < 0.0001$ compared with control) (see Table 2). Treatment with sulindac alone in the chemoprevention experiment also resulted in a significant decrease in weight gain ($P = 0.0325$ when compared with control).

REFERENCE

1. Meyer RE, Fish RE. A review of tribromoethanol anesthesia for production of genetically engineered mice and rats. *Lab Anim (NY).* 2005;34(10):47–52.